The effective electroelastic moduli of textured piezoelectric polycrystalline aggregates

Jiang Yu Li*

Center of Excellence for Advanced Materials, University of California, San Diego, La Jolla, CA, 92093-0416, USA

Abstract

The effective electroelastic moduli of textured piezoelectric polycrystalline aggregates have been modeled by the self-consistent approach and traditional Voigt-Reuss averages. The orientational averaging scheme in textured piezoelectric polycrystals has been developed using the orientation distribution function (ODF), which can be done analytically with a series of generalized associated Legendre functions, or numerically with the Gaussian quadrature method. Gaussian distribution function has been adopted to simulate a wide range of textures in piezoelectric polycrystals, and a key parameter α is identified to be closely related to the processing conditions such as poling field intensity. Numerical results are presented and discussed for poled and unpoled $BaTiO_3$ ceramics, and $BaTiO_3$ films with perfectly aligned grains, which agree well with known theoretical results. It is found that the electroelastic moduli of piezoelectric polycrystalline aggregates show strong dependence on texture; piezoelectric constants higher than the corresponding single crystal values can be achieved at certain texture; and dielectric constants are more sensitive to grain shape than elastic constants. © 2000 Elsevier Science Ltd. All rights reserved.

Keywords: Piezoelectric materials; Polycrystalline ceramics; Thin films; Electroelastic moduli; Orientation distribution

---

* Tel.: + 1-858-534-4772; fax: + 1-858-534-2727.
 E-mail address: jjli@starlite.ucsd.edu (J.Y. Li).

1. Introduction

Applications of piezoelectric materials have increased dramatically in recent years, fueled largely by their many uses in smart materials and structural systems. Their attractiveness stems from their inherent ability to convert electrical energy to mechanical energy and vice versa. They are a natural choice for ultraprecise displacement transducers and actuators. Their role in functional material systems is rapidly increasing as a result of technological trends toward higher speed, less driving power, and miniaturization of devices.

Among the piezoelectric materials, piezoelectric ceramics and thin films may have received the most attention. For contemporary and future applications, polycrystalline piezoelectric ceramics are more attractive than single crystals because they are more versatile, their physical and mechanical properties can be tailored to specific applications, they are less expensive to produce, and quality control is more easily maintained. Piezoelectric thin films are widely recognized for their potential applications in electronic and electro-optic devices. Because of their high dielectric constant and breakdown voltage, $BaTiO_3$ thin films are the best storage dielectrics for ultra-large-scale integrated memory devices. Ferroelectric PZT films show superior piezoelectric and pyroelectric properties and are used in nonvolatile memories, thermal or ultrasonic image sensors, and surface acoustic wave filters.

Despite the difference in their processing, piezoelectric ceramics and thin films can be classified as polycrystalline aggregates, with individual grains oriented with a certain distribution. So they can be analyzed under the unified framework. When a piezoelectric ceramic is fabricated by standard ceramic processing techniques, it is an aggregate of randomly oriented piezoelectric grains. No net macroscopic polarization is realized because the polarization directions are randomly oriented, and the material is not macroscopically piezoelectric. If the isotropic non-piezoelectric ceramic is subjected to a large electric field at high temperature (a process termed poling), the directions of polarization in many of the grains are permanently realigned resulting in a macroscopic spontaneous polarization and hence, piezoelectricity. The most prominent microstructural characteristic of thin films is the so-called columnar grain, i.e., highly oriented long needle-like grain. Sakashita et al. (1993) reported a fabrication of PZT thin film with the tetragonal perovskite structure and [001] texture. Stemmer et al. (1995) compared the domain configuration in epitaxial ferroelectric $PbTiO_3$ films, where domains with x_3 axis parallel and normal to the substrate surface are observed. A highly c-oriented Bismuth Titanate (BIT) film was obtained on a silver foil by Lu et al. (1996). No evidence of grain orientations other than [001] was observed for films with one- through ten-layer coating. When the number of coating layers was greater than ten, the [200] orientation was dominant. The preferential orientation in the [200] direction of BIT thin film is very attractive because the largest value of spontaneous polarization lies in the $x_1 - x_3$ plane and in the x_1 direction. In all the cases, the grain orientation distribution is very

important in determining the macroscopic behaviors of the polycrystalline aggregates.

From the above discussion on the microstructures of piezoelectric polycrystals, it is clear that texture plays an important role in their effective behaviors, and its influence can not be overemphasized. It will introduce piezoelectricity in the otherwise isotropic ceramics, and provide the optimized performance to the piezoelectric thin films. Therefore, an understanding of the effect of texture on the overall properties is very important to the design, processing, and application of piezoelectric polycrystals. Previous studies on piezoelectric ceramics have been carried out by Marutake (1956), Olson and Avellaneda (1992), and Dunn (1995). Marutake and Olson and Avellaneda were concerned with unpoled ceramics, which consist of grains having randomly oriented polar axes, and thus are isotropic and non-piezoelectric at the macroscopic level. They showed that the piezoelectric interaction at grain level significantly affects the macroscopic dielectric and elastic constants of the unpoled ceramics. Dunn considered the effect of grain shape, porosity, and microcracks on the elastic and dielectric constants of unpoled ceramics. He found that dielectric constant is more sensitive to both grain shape and grain level piezoelectric coupling. All the work focused on the elastic and dielectric moduli of unpoled and thus macroscopically non-piezoelectric ceramics, and an account of effect of texture on the macroscopic behaviors of piezoelectric ceramics is still lacking. The work on piezoelectric thin films is even more limited. Benveniste (1994) obtained exact connections between polycrystal and crystal properties in a two-dimensional piezoelectric polycrystal composed of single crystals of class 2mm. Li et al. (1999) gave the conditions for the existence of exact solutions for the effective thermal and electroelastic moduli of polycrystals exhibiting fiber texture. No attempt has been made to estimate the effective moduli of piezoelectric thin films for more general symmetries and microstructures.

In this work, we will study the effect of polycrystalline microstructure, especially the texture, on the effective behaviors of piezoelectric ceramics and thin films. As a result of their similarity in polycrystalline microstructure, they are studied under the same framework. The paper is organized in the following manner. Basic equations and notation on piezoelectricity are introduced in Section 2. Various micromechanics schemes are generalized to piezoelectric polycrystals in Section 3. The orientation distribution and orientational average are then discussed in Section 4. Finally, numerical results and discussion on BaTiO$_3$ polycrystals with general texture, BaTiO$_3$ thin films with perfect aligned grains, and isotropic BaTiO$_3$ ceramics are presented in Section 5.

2. Basic equations and notation

We consider the piezoelectric, and thus inherently anisotropic, analog of the uncoupled theory of elasticity, where the electric and elastic fields are fully coupled. The field variables and material moduli are represented either by

conventional indicial notation or by bold characters. The constitutive equation for stationary linear response of a piezoelectric solid can be expressed as

$$\sigma_p = C_{pq}\epsilon_q - e_{pk}E_k$$

$$D_i = e_{iq}\epsilon_q + \kappa_{ik}E_k \tag{1}$$

In Eq. (1) σ_p and ϵ_p are the elastic stress and strain, respectively; D_i and E_i are the electric displacement and field, respectively. C_{pq}, e_{iq}, and κ_{ik} are the elastic stiffness tensor (measured in a constant electric field), the piezoelectric tensor, and the dielectric tensor (measured at a constant strain), respectively. The well known contracted notation for tensors is adopted (Nye, 1957). We introduce the matrix representation for these quantities

$$\Sigma = \begin{bmatrix} \sigma \\ D \end{bmatrix} \quad Z = \begin{bmatrix} \epsilon \\ -E \end{bmatrix} \quad G = \begin{bmatrix} C & e^t \\ e & -\kappa \end{bmatrix} \tag{2}$$

where Σ and Z are 9×1 column vectors representing the electroelastic field variables, G is 9×9 matrix representing the electroelastic moduli, and the superscript t is used to denote the transpose of matrix. Electric field $-E$ instead of E is used as independent variable because it allows the construction of a symmetric moduli matrix, which is proven advantageous. The constitutive Eq. (1) can then be rewritten as

$$\Sigma = GZ \tag{3}$$

It is noted that the constitutive Eq. (3) is only one of four representations available for piezoelectricity. By choosing different independent field variables, other representations can be realized. The current representation is proven advantageous for the analysis of the inclusion and inhomogeneity problems, because the independent variables ϵ and $-E$ are derivable from electric potential and elastic displacement, which can be determined by the Green's function method (Dunn and Taya, 1993). This representation, however, leads to a non-positive definite energy function, piezoelectric enthalpy, which is disadvantageous in discussing the bounds on the effective moduli. In that situation, σ and E can be chosen as independent variables, leading to a positive definite energy function, and thus, upper and lower bounds on the effective moduli. Finally, we note that transformation between different representations can be done easily through the constitutive equations.

   Assuming statistical homogeneity for a heterogeneous solid subjected to external loading consistent with the uniform field Z^0 at the boundary, the effective electroelastic moduli G^* can be defined as

$$\langle \Sigma \rangle = G^* \langle Z \rangle, \tag{4}$$

where $\langle \bullet \rangle = \int (\bullet) d\Omega(\theta, \varphi, \phi)$ denotes an orientational volume average, in which (θ, φ, ϕ) are Euler angles describing the orientation of a grain $O-X_1X_2X_3$ in a global

coordinate system $O-x_1x_2x_3$ depicted in Fig. 1 (see, for example, Roe, 1965). Due to linearity we have

$$Z(\theta, \varphi, \phi) = A(\theta, \varphi, \phi)Z^0 \tag{5}$$

where $A(\theta, \varphi, \phi)$ is the concentration factor for grain at orientation (θ, φ, ϕ), which is a function of microstructure parameters, such as grain shape, orientation, and interaction between different grains. From the average field theorem (Dunn and Taya, 1993; Hori and Nemat-Nasser, 1998), i.e., $\langle Z(\theta, \varphi, \phi) \rangle = Z^0$, we can show that

$$\langle A(\theta, \varphi, \phi) \rangle = I, \tag{6}$$

where I is the 9×9 unit matrix. Inserting Eq. (5) into Eq. (4), combined with the constitutive Eq. (3) for individual grains at different orientations, and after some manipulation, we have

$$G^* = \langle G(\theta, \varphi, \phi)A(\theta, \varphi, \phi) \rangle, \tag{7}$$

where $G(\theta, \varphi, \phi)$ are the electroelastic moduli of grain at orientation (θ, φ, ϕ) expressed in the global coordinate system. Eq. (7) is an exact expression that rigorously connects the effective moduli of the polycrystal with electroelastic
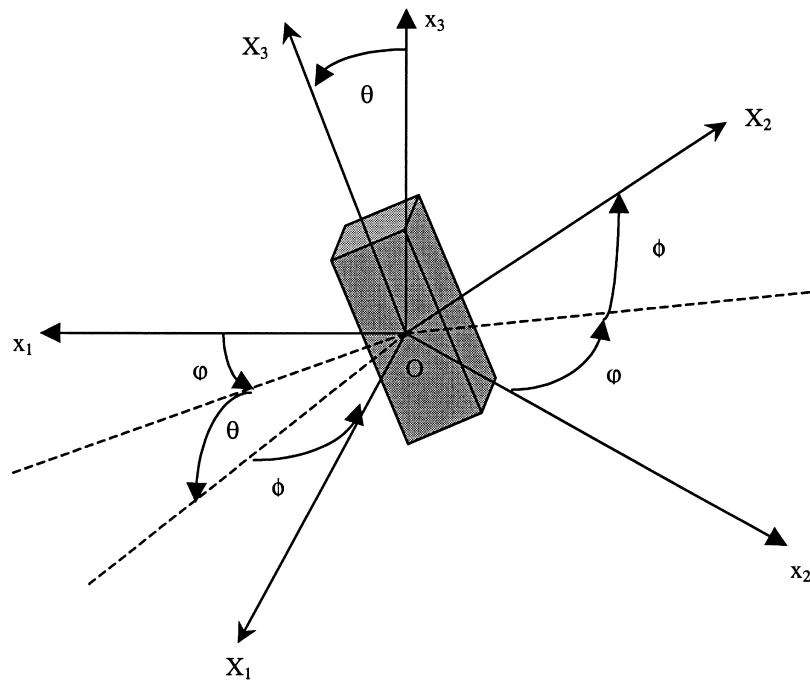
Fig. 1. Euler angles (θ, φ, ϕ) for a grain in a global coordinate system.

moduli and concentration factors of individual grains. It is clear from Eq. (7) that the estimation of effective electroelastic moduli depends on the estimation of the concentration factor $A(\theta, \varphi, \phi)$, which is the starting point of various micromechanics approximations.

3. Micromechanics schemes

The simplest assumption on the concentration factor is $A(\theta, \varphi, \phi) = I$. This corresponds to assuming uniform stress and electric field in the polycrystal subjected to an external loading, and gives us

$$G^* = \langle G(\theta, \varphi, \phi) \rangle \tag{8}$$

Analogously, by assuming $\Sigma(\theta, \varphi, \phi) = B(\theta, \varphi, \phi)\Sigma^0$, and letting $B(\theta, \varphi, \phi) = I$, a uniform strain and electric displacement assumption, we obtain

$$G^* = \langle G^{-1}(\theta, \varphi, \phi) \rangle^{-1} \tag{9}$$

Eqs. (8) and (9) are the piezoelectric analogs of Voigt-Reuss averages in elastic solids (Voigt, 1889; Reuss, 1929). As noted in Section 2, the matrix of electroelastic moduli G is not positive definite, and Voigt-Reuss estimations do not provide upper and lower bounds on the electroelastic moduli. For the discussions on the variational bounds for piezoelectric composite, readers are referred to Bisegna and Luciano (1996), Hori and Nemat-Nasser (1998), and Li and Dunn (1998a), in which different independent field variables are chosen. Recently Li et al. (1999) showed that the uniform fields exist in piezoelectric polycrystals with fiber texture under certain conditions, so that Voigt-Reuss estimations are exact for some components of the electroelastic moduli. In general, however, the uniform field assumption is not realistic, especially in the case of strong grain anisotropy, such as piezoelectric crystals. So a more elaborate micromechanics scheme is needed to model the effective behaviors of piezoelectric polycrystals.

It is obvious that the estimation of concentration factor A is equivalent to the estimation of the electroelastic fields in individual grains of polycrystal subjected to external loading Z^0 at the boundary. To this end we turn to the Eshelby solution on inclusion and inhomogeneity problems (Dunn and Taya, 1993; Eshelby, 1957), and the self-consistent assumption (Dunn, 1995; Walpole, 1969; Willis, 1977). We assume that the individual grains are embedded in an infinite matrix with yet to be determined effective electroelastic moduli G^*, subjected to the yet to be determined external loading Z_1 at the boundary. It follows that

$$Z(\theta, \varphi, \phi) = A^{dil}(\theta, \varphi, \phi)Z_1 \tag{10}$$

where $A^{dil}(\theta, \varphi, \phi)$ is determined from the solution of a single inhomogeneity embedded in an infinite matrix (Dunn and Taya, 1993)

$$A^{dil}(\theta, \varphi, \phi) = \{I + S(\theta, \varphi, \phi)G^{*-1}[G(\theta, \varphi, \phi) - G^*]\}^{-1} \tag{11}$$

where $S(\theta, \varphi, \phi)$ is the piezoelectric Eshelby tensor for grain at orientation (θ, φ, ϕ) expressed in the global coordinate system, which is a function of the effective electroelastic moduli G^* of the matrix and the grain shape. We will discuss the evaluation of the piezoelectric Eshelby tensor in Appendix A. For an aligned spheroidal inclusion in a transversely isotropic matrix, there are closed form expressions for Eshelby tensor available (Dunn and Wienecke, 1997; Li and Dunn, 1998b). For the more general case, it is necessary to evaluate the Eshelby tensor numerically. From the average field theorem it follows from Eq. (10) that

$$Z_1 = \langle A^{dil}(\theta, \varphi, \phi) \rangle^{-1} Z^0 \tag{12}$$

And finally we obtain

$$A(\theta, \varphi, \phi) = A^{dil}(\theta, \varphi, \phi)\langle A^{dil}(\theta, \varphi, \phi) \rangle^{-1} \tag{13}$$

and

$$G^* = \langle G(\theta, \varphi, \phi)(A^{dil}(\theta, \varphi, \phi)) \rangle \langle A^{dil}(\theta, \varphi, \phi) \rangle^{-1}. \tag{14}$$

Since G^* is involved in both sides of equation, in general, Eq. (14) can only be solved numerically by iteration. Eq. (14) is recognized as a self-consistent approach, and regarded as an effective medium assumption. From our derivation, however, it clearly also has the nature of an effective field assumption besides the effective medium origin (see also Li (1999) for more discussion). One of the problems for the application of micromechanics models in multi-phase composites is the violation of diagonal symmetry, as demonstrated by Benveniste et al. (1991). The self-consistent model we developed here does not have such a problem. It always returns a diagonally symmetric moduli matrix as verified by our numerical calculations. It will also be interesting to see if the effective moduli predicted by Eq. (14) fall between variational bounds or not. However, since the Hashin-Shtrikman type of bounds (Hashin and Shtrikman, 1962, 1963; Willis, 1977) for piezoelectric polycrystals is still under development, such evaluation is not possible at this moment, and will be reported later.

4. Orientation distribution function and orientational average

It is clear from Eqs. (8), (9), and (14) that the estimation of the effective electroelastic moduli of piezoelectric polycrystals involves orientational volume averages, no matter which micromechanics scheme is used. The orientation distribution of grains in the polycrystal can be described by the orientation distribution function (ODF) $W(\xi, \varphi, \phi)$, which is the probability density function for a grain at orientation (θ, φ, ϕ), where $\xi = \cos\theta$, and (θ, φ, ϕ) are Euler angles describing the grain's orientation with respect to a global sample coordinate system (Roe, 1965), see Fig. 1. The orientational volume average of a single
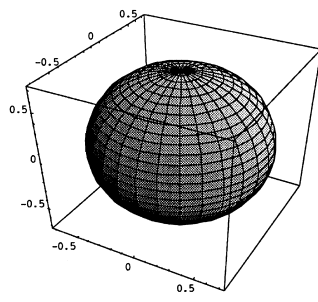
lmn=000
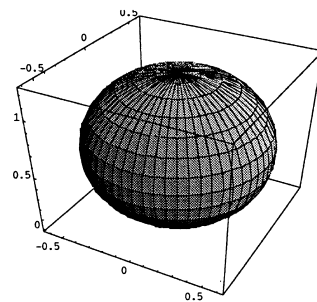
lmn=100
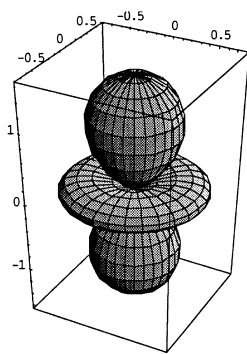
lmn=200
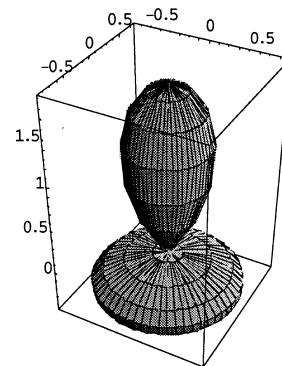
lmn=300
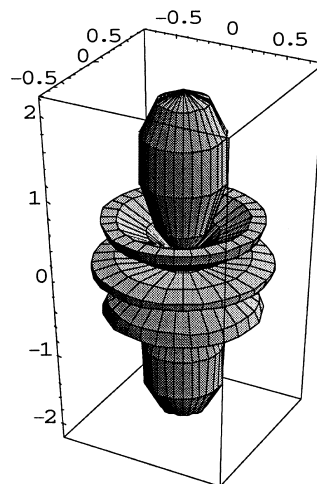
lmn=400

Fig. 2. Nonzero basis function $Z_{lmn}(\xi)e^{-im\varphi}e^{-in\phi}$.

crystal tensorial property H weighted by ODF is then given by

$$\langle H \rangle = \int_0^{2\pi} \int_0^{2\pi} \int_{-1}^1 H(\xi, \varphi, \phi) W(\xi, \varphi, \phi) d\xi d\varphi d\phi \tag{15}$$

where $H(\xi, \varphi, \phi)$ is the single crystal value of H expressed in the global coordinate system. To evaluate $\langle H \rangle$, we expand $W(\xi, \varphi, \phi)$ and $H(\xi, \varphi, \phi)$ into series of generalized associated Legendre functions

$$W(\xi, \varphi, \phi) = \sum_{l=0}^{l=\infty} \sum_{m=-l}^{l} \sum_{n=-l}^{l} W_{lmn} Z_{lmn}(\xi) e^{-im\varphi} e^{-in\phi} \tag{16}$$

$$H(\xi, \varphi, \phi) = \sum_{l=0}^{l=\infty} \sum_{m=-l}^{m=l} \sum_{n=-l}^{n=l} H_{lmn} Z_{lmn}(\xi) e^{-im\varphi} e^{-in\phi} \tag{17}$$

where $Z_{lmn}(\xi)$ is the generalized associated Legendre function, and can be expressed in terms of ordinary functions and the common Legendre function $P_l^{mn}(\xi)$ as (Bunge, 1982)

$$Z_{lmn}(\xi) = i^{n-m} \sqrt{\frac{2l+1}{2}} P_l^{mn}(\xi)$$

with

$$P_l^{mn}(\xi) = \frac{(-1)^{l-m} i^{n-m}}{2^l (l-m)!} \left[\frac{(l-m)!(l+n)!}{(l+m)!(l-n)!} \right]^{\frac{1}{2}}$$

$$\times \frac{(1-\xi)^{\frac{-(n-m)}{2}}}{(1+\xi)^{\frac{(n+m)}{2}}} \frac{d^{l-n}}{d\xi^{l-n}}[(l-\xi)^{l-m}(l+\xi)^{l+m}]$$

where $i^2 = -1$. Care should be taken to avoid confusion between electroelastic field Z and generalized associated Legendre function $Z_{lmn}(\xi)$, which should be clear from the context. To help visualize, we plot some nonzero basis functions $Z_{lmn}(\xi) e^{-im\varphi} e^{-in\phi}$ in Fig. 2. Due to orthogonality, the expansion coefficients can be expressed as follows

$$W_{lmn} = \frac{1}{4\pi^2} \int_0^{2\pi} \int_0^{2\pi} \int_{-1}^1 W(\xi, \varphi, \phi) Z_{lmn}(\xi) e^{im\varphi} e^{in\phi} d\xi d\varphi d\phi \tag{18}$$

$$H_{lmn} = \frac{1}{4\pi^2} \int_0^{2\pi} \int_0^{2\pi} \int_{-1}^1 H(\xi, \varphi, \phi) Z_{lmn}(\xi) e^{im\varphi} e^{in\phi} d\xi d\varphi d\phi \tag{19}$$

The texture coefficients W_{lmn} represent the orientation distribution of grains in the polycrystalline aggregate. By the normalization condition for the ODF we can

show that

$$W_{000} = \frac{1}{4\sqrt{2}\pi^2}$$

Even-rank texture coefficients can be determined from X-ray diffraction intensity, which was discussed in detail by Roe (1965). Such a technique is not able to give any information on odd-rank texture coefficients, due to the inherent centrosymmetry in X-ray diffraction. It is hoped that the present work can provide a potential method to determine the odd-rank texture coefficients inversely from the measurement of odd-rank tensorial properties, such as piezoelectric constants. Using Eqs. (16) and (17), and taking into account the orthogonal property of $Z_{lmn}(\xi)$, we can reduce Eq. (15) to

$$\langle H \rangle = 4\pi^2 \sum_{l=0}^{R} \sum_{m=-l}^{l} \sum_{n=-l}^{l} H_{lmn} W_{lmn} \tag{20}$$

Where R is the rank of tensorial property H. Only the first R terms in the series expansion need to be considered in averaging a tensorial property of rank R (Ferrari and Johnson, 1988).

We now consider the polycrystalline aggregates composed of 4 mm single crystals, for example, BaTiO$_3$. The independent single crystal moduli would be elastic constants C_{11}, C_{12}, C_{13}, C_{33}, C_{44}, and C_{66}, piezoelectric constants e_{15}, e_{31}, and e_{33}, and dielectric constants κ_{11}, and κ_{33}. The resulting polycrystal is transversely isotropic with

$$\langle C_{66} \rangle = \frac{\langle C_{11} \rangle - \langle C_{12} \rangle}{2},$$

and the only non-zero texture coefficients are W_{100}, W_{200}, W_{300}, W_{400}, and W_{404}. Unlike Roe's original treatment, we have nonzero odd-rank texture coefficients W_{100} and W_{300} due to lack of centrosymmetry in piezoelectric materials. From Eqs. (18) and (19) it follows that the orientational averages for 4th, 3rd, and 2nd rank tensorial properties can be deduced from the following tensor transformation laws

$$\langle C_{ijkl}(\xi, \varphi, \phi) \rangle = \langle T_{im} T_{jn} T_{ko} T_{lp} C_{mnop} \rangle = \langle T_{im} T_{jn} T_{ko} T_{lp} \rangle C_{mnop} \tag{21a}$$

$$\langle e_{ijk}(\xi, \varphi, \phi) \rangle = \langle T_{im} T_{jn} T_{ko} e_{mno} \rangle = \langle T_{im} T_{jn} T_{ko} \rangle e_{mno} \tag{21b}$$

$$\langle \kappa_{ij}(\xi, \varphi, \phi) \rangle = \langle T_{im} T_{jn} K_{mn} \rangle = \langle T_{im} T_{jn} \rangle K_{mn} \tag{21c}$$

where T_{mn} is the element of tensor transformation matrix in terms of Euler angles,

$$T^{-1} = \begin{bmatrix} \cos\varphi\cos\theta\cos\phi - \sin\varphi\sin\phi & \sin\varphi\cos\theta\cos\phi + \cos\varphi\sin\phi & -\sin\theta\cos\phi \\ -\cos\varphi\cos\theta\sin\phi - \sin\varphi\sin\phi & -\sin\varphi\cos\theta\sin\phi + \cos\varphi\cos\psi & \sin\theta\sin\phi \\ \cos\varphi\sin\theta & \sin\varphi\sin\theta & \cos\theta \end{bmatrix}$$

(22)

After expanding the $\langle\bullet\rangle$ terms in Eqs. (21) into series, and determining their coefficients according to Eq. (19), we are able to obtain the following expressions for the orientational averages for 4th, 3rd, and 2nd rank tensorial properties using Eq. (20).

4.1. Fourth rank tensor: elastic constants

$$\langle C_{11}\rangle = C_{11}^0 + aW_{200} + 3bW_{400} + jW_{404}$$

$$\langle C_{12}\rangle = C_{12}^0 + 2cW_{200} + bW_{400} + jW_{404}$$

$$\langle C_{13}\rangle = C_{12}^0 - cW_{200} - 4bW_{400} - 4jW_{404}$$

$$\langle C_{33}\rangle = C_{11}^0 - 2aW_{200} + 8bW_{400} + 8jW_{404}$$

$$\langle C_{44}\rangle = \frac{C_{11}^0 - C_{12}^0}{2} - \frac{a - 2c}{4}W_{200} - 4bW_{400} - 4jW_{404}$$

where

$$C_{11}^0 = (6C_{11} + 2C_{12} + 4C_{13} + 3C_{33} + 8C_{44} + 4C_{66})/15$$

$$C_{12}^0 = (2C_{11} + 4C_{12} + 8C_{13} + C_{33} - 4C_{44} - 2C_{66})/15$$

$$a = 8\sqrt{10}\pi^2(3C_{11} + C_{12} - C_{13} - 3C_{33} - 2C_{44} + 2C_{66})/105$$

$$b = \sqrt{2}\pi^2(3C_{11} + C_{12} - 8C_{13} + 4C_{33} - 16C_{44} + 2C_{66})/105$$

$$c = 4\sqrt{10}\pi^2(C_{11} + 5C_{12} - 5C_{13} - C_{33} + 4C_{44} - 4C_{66})/105$$

$$j = 2\sqrt{35}\pi^2(C_{11} - C_{12} - 2C_{66})/105$$

4.2. Third rank tensor: piezoelectric constants

$$\langle e_{15} \rangle = \frac{4\sqrt{6}\pi^2}{15}(3e_{15} - e_{31} + e_{33})W_{100} + \frac{4\sqrt{14}\pi^2}{35}(2e_{15} + e_{31} - e_{33})W_{300}$$

$$\langle e_{31} \rangle = \frac{4\sqrt{6}\pi^2}{15}(-2e_{15} + 4e_{31} + e_{33})W_{100} + \frac{4\sqrt{14}\pi^2}{35}(2e_{15} + e_{31} - e_{33})W_{300}$$

$$\langle e_{33} \rangle = \frac{4\sqrt{6}\pi^2}{15}(4e_{15} + 2e_{31} + 3e_{33})W_{100} - \frac{8\sqrt{14}\pi^2}{35}(2e_{15} + e_{31} - e_{33})W_{300}$$

4.3. Second rank tensor: dielectric constants

$$\langle \kappa_{11} \rangle = \frac{2\kappa_{11} + \kappa_{33}}{3} + \frac{4\sqrt{10}\pi^2}{15}(\kappa_{11} - \kappa_{33})W_{200}$$

$$\langle \kappa_{33} \rangle = \frac{2\kappa_{11} + \kappa_{33}}{3} - \frac{8\sqrt{10}\pi^2}{15}(\kappa_{11} - \kappa_{33})W_{200}$$

It is noted that the elastic constants only depend on W_{200}, W_{400} and W_{404}, piezoelectric constants only depend on W_{100} and W_{300}, and dielectric constants only depend on W_{200}. When all these texture coefficients are zero, the material becomes isotropic, and there is no piezoelectric effect. Materials with centrosymmetry will also show no piezoelectricity, since their W_{100} and W_{300} are zero.

The orientational averaging scheme presented is based on the fact that the tensorial properties in different grains at different orientations are identical in their own local coordinate systems, as is clear from Eq. (21). This is true for the electroelastic moduli G and G^{-1}, so Voigt-Reuss estimations (8) and (9) can be evaluated using this scheme. It is no longer true, however, for the concentration factor A, because A is not a material property and varies between different orientations. Therefore, the orientational averaging scheme we presented can not be applied to the concentration factor A and the self-consistent approach (14). In general, the dependence of the concentration factor A on the orientation is very complicated and no analytic solution is available, so Eqs. (19) and (20) are no longer applicable, and we must turn to the original Eq. (15) for orientational averaging of the concentration factor A and the self-consistent approach (14). The disadvantage of Eq. (15) is that the ODF $W(\xi, \varphi, \phi)$, unlike the texture coefficients W_{lmn}, is not experimental measurable. In principle, however, we can determine W_{lmn} from experiment, and fit the ODF $W(\xi, \varphi, \phi)$ with the restrictions of Eq. (18). The other problem is that unlike the algebraic Eq. (20), Eq. (15) contains an integration involving the complicated function $A(\xi, \varphi, \phi)$, which can

only be evaluated numerically in general. Nevertheless, it can still be solved with high accuracy, for example, by the Gaussian quadrature method (Press et al., 1992).

5. Numerical results and discussion

To demonstrate the applicability of the theory, we will show some numerical results in this Section. Since there is no experimental measurement on texture available for piezoelectric polycrystals, to the best knowledge of the author, we will adopt the Gaussian distribution function as ODF, which turns out to be a reasonable approximation. Because the piezoelectric polycrystals are usually transversely isotropic, we assume that the distribution only depends on Euler angle θ and is not a function of φ and ϕ

$$W(\theta, \varphi, \phi) = \frac{1}{\alpha\sqrt{2\pi}} Exp\left(-\frac{\theta^2}{2\alpha^2} \right) \tag{23}$$

where α is a parameter in Gaussian distribution function, and can be adjusted to give different texture. The shape of the Gaussian distribution function with various α is shown in Fig. 3. The non-zero W_{lmn} as a function of α is shown in Fig. 4. Since the ODF does not depend on ϕ, W_{404} is also zero. Two extreme cases immediately follow from the Gaussian distribution, where a polycrystal with perfectly aligned grains such as a piezoelectric thin film is realized by letting $\alpha \to 0$, and randomly oriented isotropic ceramics (unpoled) is realized by letting
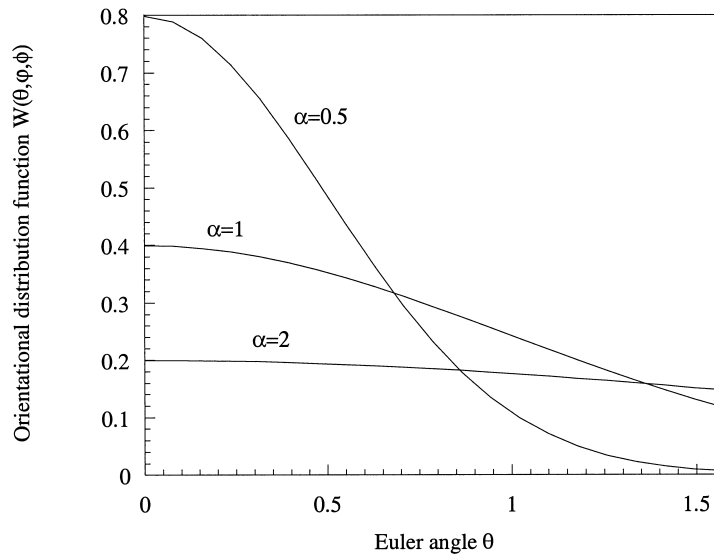
Fig. 3. Gaussian distribution function with different parameters α.
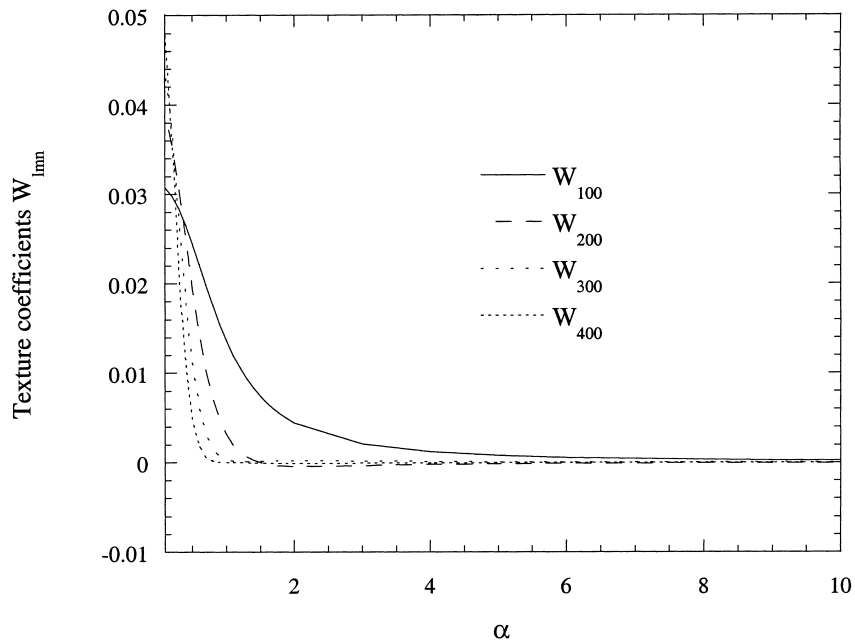
Fig. 4. Texture coefficients W_{lmn} as functions of Gaussian distribution function parameter α.

$\alpha \to \infty$. Other texture can be realized by varying α in between. It can be imagined that α is closely related to the processing conditions of piezoelectric polycrystals, such as poling field intensity. The ceramics are isotropic without poling field applied, and α approaches infinity. When an electric field is applied in poling, some grains will reorient to minimize the free energy of the system, and α takes some finite value, depending on the magnitude of the poling field. At saturation field all the grains are perfectly aligned with polarization along the poling field direction, and α approaches zero. By an appropriate experimentation the relationship between α and processing conditions can be identified, but that line of inquiry will not be pursued here.

We apply the theory to $BaTiO_3$ polycrystals, where the material constants are listed in Table 1 (Berlincourt and Jaffe, 1958). The Gaussian quadrature method is adopted for numerical integration (Press et al., 1992), where the integral of a

Table 1
Electroelastic constants of tetragonal $BaTiO_3$ single crystal

C_{11} (GPa)	C_{12} (GPa)	C_{13} (GPa)	C_{33} (GPa)	C_{44} (GPa)	C_{66} (GPa)
275.1	178.9	151.55	164.8	54.3	113.1
$e_{31}(C/m^2)$	$e_{33}(C/m^2)$	$e_{15}(C/m^2)$	κ_{11}/κ^0	κ_{33}/κ^0	
−2.69	3.65	21.3	1970	109	

Table 2
Procedures for self-consistent calculation of effective electroelastic constants

1. Input the effective electroelastic constants of single crystal BaTiO$_3$ and parameter α of Gaussian distribution function, and pre-determined number of abscissas to be evaluated in Gaussian quadratures method.
2. Determine a set of orientations $(\theta_j, \varphi_j, \phi_j)$ as abscissas, and the corresponding weighting coefficient w_j.
3. Compute an initial guess for the current effective electroelastic moduli by Voigt estimations: $G^i = \langle G \rangle$.
4. Set the initial $\langle A^{dil} \rangle_j^i$ and $\langle GA^{dil} \rangle_j^i$ to be zero.
5. Transform the current effective moduli G^i to local coordinate system $(\theta_j, \varphi_j, \phi_j)$.
6. Compute Eshelby tensor S_j^i at the local coordinate system $(\theta_j, \varphi_j, \phi_j)$ from the current effective electroelastic moduli G^i.
7. Compute the dilute concentration factors $A^{dil}(\theta_j, \varphi_j, \phi_j)$ and $GA^{dil}(\theta_j, \varphi_j, \phi_j)$ at the local system from Eq. (11), and transform them to global coordinate system.
8. Compute orientational averages $\langle A^{dil} \rangle_{j+1}^i = \langle A^{dil} \rangle_j^i + w_j A^{dil}(\theta_j, \varphi_j, \phi_j)$ and $\langle GA^{dil} \rangle_{j+1}^i = \langle GA^{dil} \rangle_j^i + w_j G(\theta_j, \varphi_j, \phi_j) A^{dil}(\theta_j, \varphi_j, \phi_j)$.
9. Repeat steps 5–8 until all the abscissas are included.
10. Compute an updated estimate of current effective moduli G^{i+1} from Eq. (14).
11. Repeat steps 4–10 until converge condition is satisfied.

function is approximated by the sum of its function values at a set of points called abscissas, multiplied by weighting coefficients. The calculation is implemented in a FORTRAN code, with the procedure outlined in Table 2, where the superscript i is used to indicate the step in the iteration of the self-consistent approach, and subscript j is used to indicate the step in the numerical integration, under the same step i of the self-consistent approach. Three different cases have been considered under such a scheme.

5.1. Piezoelectric polycrystals with texture

We first apply the theory to $BaTiO_3$ polycrystal with texture described by Gaussian distribution, with grains assumed to be spherical. Figs. 5–7 show the effective elastic constants, piezoelectric constants, and dielectric constants of $BaTiO_3$ polycrystal as functions of α, where α is the parameter in Gaussian distribution function. When α approaches zero, the grains in the polycrystal become perfectly aligned. In such a case Li et al. (1999) showed that the elastic constants C_{13}, C_{33}, and C_{44}, and all piezoelectric and dielectric constants of polycrystalline aggregate are exact and recover the corresponding single crystal values. It is found in the figures that the Voigt-Reuss averages and self-consistent approach agree with each other and recover the single crystal values for these moduli. This observation supports the use of the self-consistent approach and the Gaussian quadrature method. For elastic constants C_{11} and C_{66}, where no exact
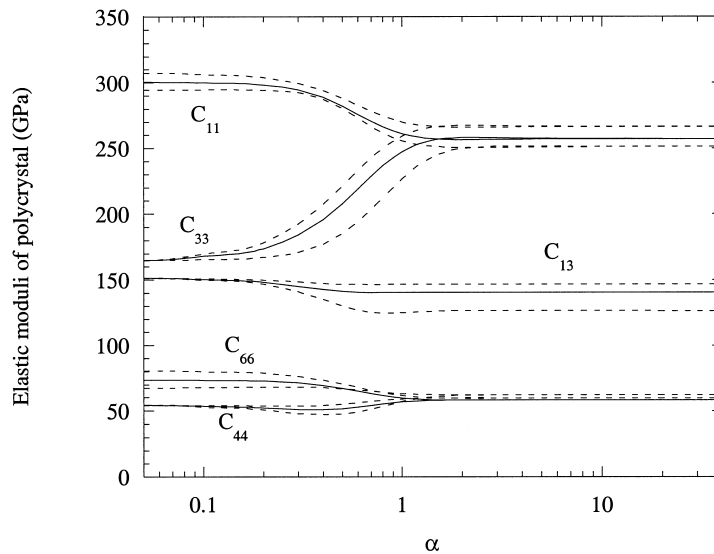
Fig. 5. Effective elastic moduli of piezoelectric polycrystal as functions of Gaussian distribution function parameter α. Solid line is the self-consistent approach, and the broken line is Voigt-Reuss averages.
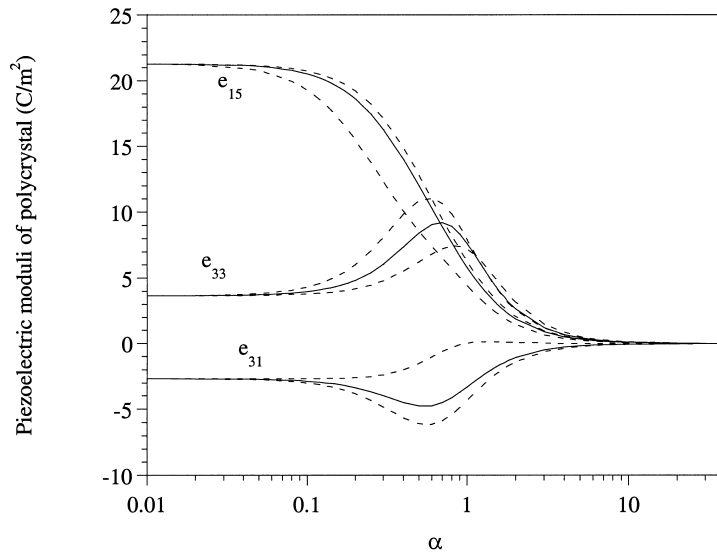
Fig. 6. Effective piezoelectric moduli of piezoelectric polycrystal as functions of Gaussian distribution function parameter α. Solid line is the self-consistent approach, and the broken line is Voigt-Reuss averages.
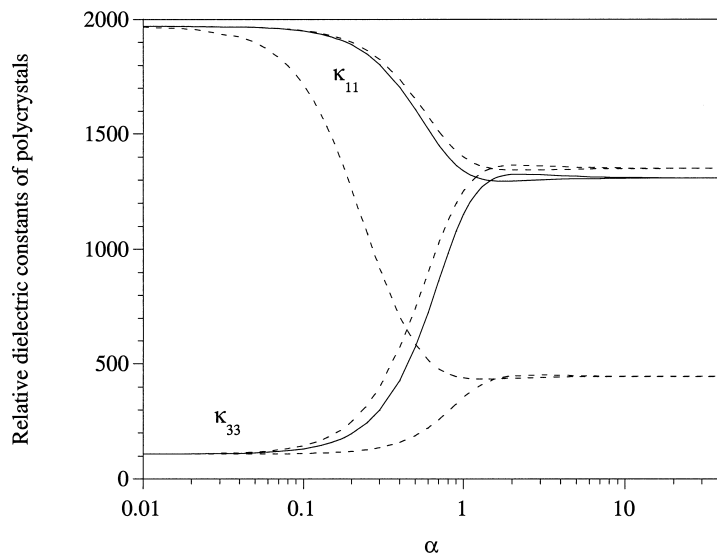
Fig. 7. Effective dielectric moduli of piezoelectric polycrystal as functions of Gaussian distribution function parameter α. Solid line is the self-consistent approach, and the broken line is Voigt-Reuss averages.

solution exists, the self-consistent approach lies between the Voigt-Reuss averages. When α approaches infinity, the ceramics become isotropic and non-piezoelectric. It is found in the figures that all piezoelectric constants become zero, and C_{11} and C_{33}, C_{44} and C_{66}, and κ_{11} and κ_{33} agree with each other, as specified by isotropic symmetry. Between these two extreme cases, the effective electroelastic moduli show strong dependency on α, thus on texture, and poling field. Two observations deserve discussion. First, there are peaks in the piezoelectric constants e_{31} and e_{33} when α approaches 0.6–0.7, which show larger magnitude than their single crystal values. This might be used to enhance the piezoelectric coupling in the ceramics. Second, when α approaches 1.5, the elastic constant C_{33} becomes a little bit larger than C_{11}, so does the dielectric constant κ_{33} compared with κ_{11}. This is in contrast with the single crystal where C_{11} and C_{11} are significantly larger. These observations can be explained in the context of the orientational average. From the Voigt average in Section 4, we know that

$$\langle e_{31} \rangle = \frac{4\sqrt{6}\pi^2}{15}(-2e_{15} + 4e_{31} + e_{33})W_{100} + \frac{4\sqrt{14}\pi^2}{35}(2e_{15} + e_{31} - e_{33})W_{300}$$

$$\langle e_{33} \rangle = \frac{4\sqrt{6}\pi^2}{15}(4e_{15} + 2e_{31} + 3e_{33})W_{100} - \frac{8\sqrt{14}\pi^2}{35}(2e_{15} + e_{31} - e_{33})W_{300}$$

Since the coefficient of W_{300} for e_{33} is negative while the coefficient of W_{100} for e_{33} is positive, and W_{300} decreases much faster than W_{100} with the increase of α (see
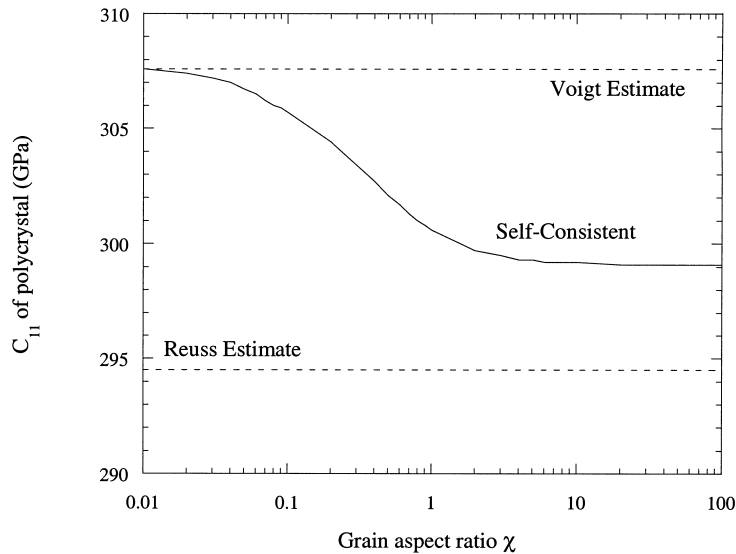
Fig. 8. Effective elastic modulus C_{11} of piezoelectric polycrystal with perfectly aligned grains as function of grain shape aspect ratio χ.

Fig. 4), there is a peak for e_{33}. A similar argument explains the peak in e_{31}. For C_{33} and C_{11}, from the Voigt average in Section 4, we know that

$$\langle C_{11} - C_{33} \rangle = 3aW_{200} - 5bW_{400}$$

Where a is positive and b is negative, and a is much larger than b in magnitude. Remember that W_{404} is zero under the Gaussian distribution. When α approaches 1.5, W_{200} becomes negative (see Fig. 4) and C_{33} becomes a little bit larger than C_{11}. A similar argument explains why κ_{33} is larger than κ_{11} when α approaches 1.5.

5.2. Piezoelectric polycrystal with perfect aligned grains

For polycrystals with all the BaTiO$_3$ grains perfectly aligned in the x_3 axis ($\alpha = 0$), for example, BaTiO$_3$ thin films with columnar grains, Li et al. (1999) have shown that the effective electroelastic moduli of polycrystals are exact, and recover the single crystal values, except for C_{11} and C_{66}. Our calculations confirm this observation and show that the self-consistent approach recovers the exact solutions in this case. Figs. 8 and 9 show the effective elastic constants C_{11} and C_{66} of a perfectly aligned BaTiO$_3$ polycrystal as function of grain shape, where spheroidal grains with aspect ratio $\chi = a_3/a_1$ are assumed. All other moduli recover the single crystal values regardless of grain shapes. It is found that the C_{11} and C_{66} are not very sensitive to grain shape, changing less than 10% with respect to
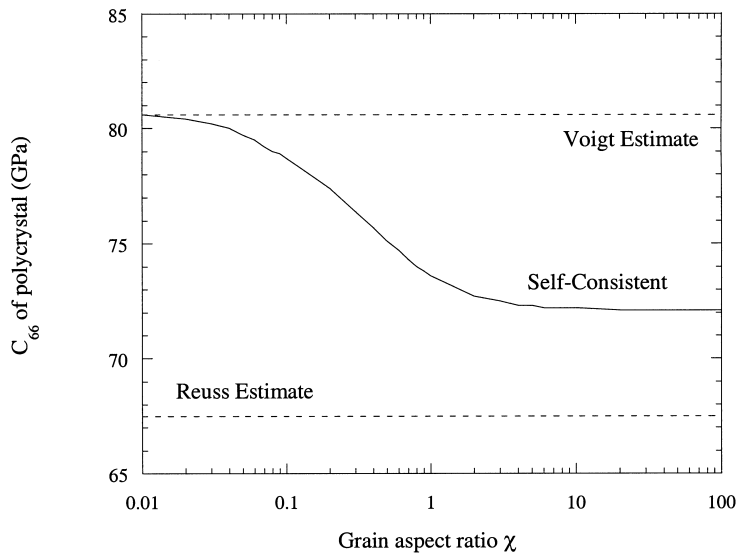
Fig. 9. Effective elastic modulus C_{66} of piezoelectric polycrystal with perfectly aligned grains as function of grain shape aspect ratio χ.

the change of grain from penny-shape to needle-shape. Both moduli are highest for penny-shaped grains, and decrease monotonically with the increase of grain shape aspect ratio, reaching a minimum when the grains become needle-shaped. It is noted that Voigt-Reuss averages are unable to model the effect of grain shapes.

5.3. Isotropic piezoelectric polycrystals

Polycrystalline ceramics with randomly oriented $BaTiO_3$ grains ($\alpha \rightarrow \infty$) are isotropic and non-piezoelectric. In this case, the independent overall properties would be bulk modulus K, shear modulus G, and dielectric constant κ. Dunn (1995) analyzed this class of materials using an exact orientational averaging scheme, taking advantage of isotropic symmetry. Our calculations, presented in Figs. 10–12, agree with his results, which supports the use of the Gaussian quadrature method in the orientational averaging. A larger range of grain aspect ratio is considered here. Again, it is observed that the effective elastic constants show weak dependency on the grain shape. The dielectric constant, however, strongly depends on the grain shape, which is a minimum for penny-shaped grains, increases monotonically with increment of grain aspect ratio, and reaches a maximum for needle-shaped grains. The changes of bulk and shear moduli are not monotonic, and reach a minimum when the grain aspect ratio is around 0.3–0.4. The stronger dependence of dielectric constants on grain shape is believed to be caused by the stronger grain anisotropy in the dielectric constants, as shown in Table 1.
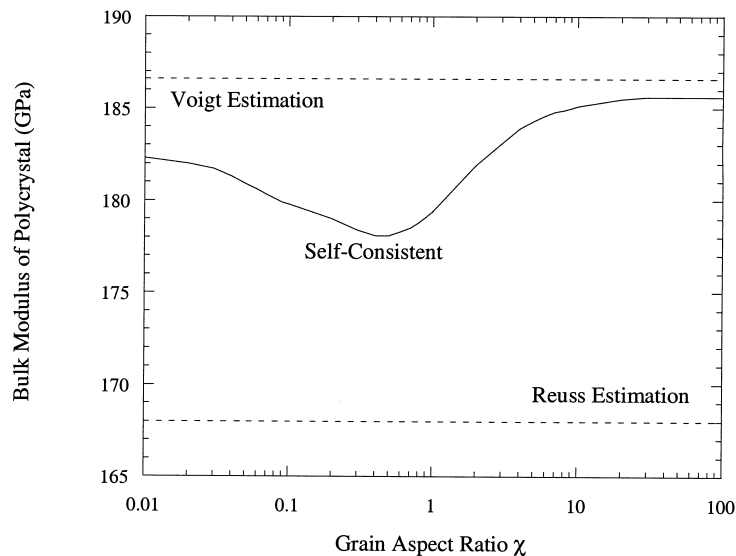
Fig. 10. Effective bulk modulus K of piezoelectric polycrystal with randomly aligned grains as function of grain shape aspect ratio χ.
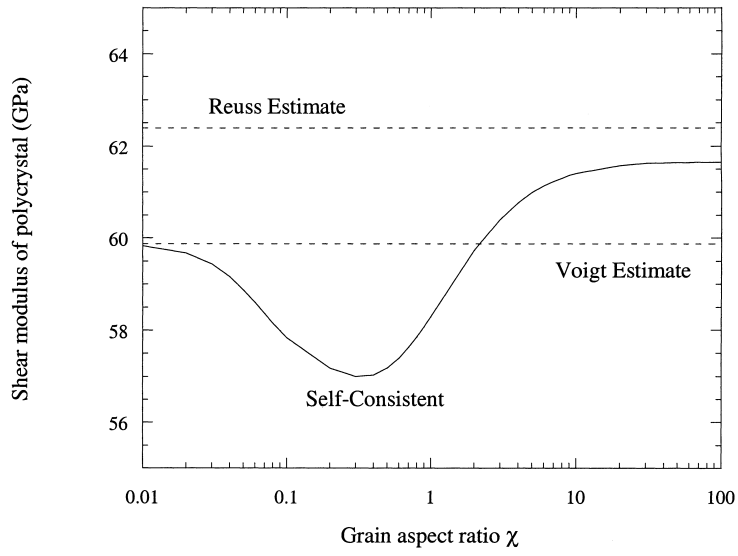
Fig. 11. Effective shear modulus *G* of piezoelectric polycrystal with randomly aligned grains as function of grain shape aspect ratio χ.
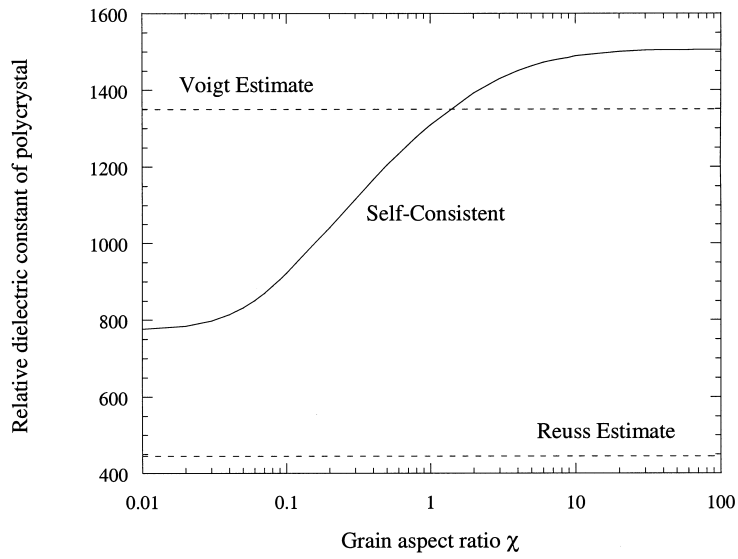
Fig. 12. Effective relative dielectric constant κ of piezoelectric polycrystal with randomly aligned grains as function of grain shape aspect ratio χ.

6. Conclusion

The self-consistent approach and traditional Voigt-Reuss estimations have been generalized to model electroelastic moduli of piezoelectric polycrystals with texture. An orientational averaging scheme has been developed using the orientation distribution function, which is approximated by a Gaussian distribution function, enabling simulation of a wide range of textures in polycrystals. Numerical results on $BaTiO_3$ polycrystals have also been presented using the Gaussian quadrature numerical integration method, which agree with theoretical results in special cases. It is found that the electroelastic moduli of piezoelectric polycrystalline aggregates show strong dependence on texture. Piezoelectric constants higher than single crystal values can be achieved at certain texture. And the dielectric constants are more sensitive to grain shape than the elastic constants due to stronger grain anisotropy.

Appendix A

Piezoelectric Eshelby tensor

Let us consider an ellipsoidal inclusion undergoing a uniform eigenfield Z_{Mn}^T, embedded in an infinite homogeneous piezoelectric solid. In the presence of the eigenfield, the constitutive equation for the inclusion is

$$\Sigma_{iJ} = G_{iJKl}(Z_{Kl} - Z_{Kl}^T) \tag{A1}$$

It has been shown that in such a situation, the electroelastic fields in the inclusion are uniform, and can be expressed as (Dunn and Taya, 1993)

$$Z_{Mn} = S_{MnAb}Z_{Ab}^T \tag{A2}$$

where S_{MnAb} is the piezoelectric Eshelby tensor, whose components are functions of the electroelastic moduli of the matrix, and the ellipsoidal shape of the inclusion. For general inclusion shapes and material symmetries, Eshelby tensors can be expressed as surface integrals over a unit sphere

$$S_{MnAb} = \frac{G_{iJAb}}{4\pi} \begin{cases} \dfrac{1}{2}\displaystyle\int_{-1}^{1}\int_{0}^{2\pi}[J_{mJin}(z) + J_{nJim}(z)]d\theta d\xi_3 & M = 1,\,2,\,3 \\[2ex] \displaystyle\int_{-1}^{1}\int_{0}^{2\pi} J_{4Jin}(z)d\theta d\xi_3 & M = 4 \end{cases} \tag{A3}$$

In Eq. (A3) $z_i = \xi_i/a_i$ (no sum on i), where a_i is the dimension of the ellipsoidal axis, and ξ_1 and ξ_2 can be expressed in terms of ξ_3 and θ by $\xi_1 = \sqrt{1 - \xi_3^2}\cos\theta$ and $\xi_1 = \sqrt{1 - \xi_3^2}\sin\theta$. In addition, $J_{MJin} = z_i z_n K_{MJ}^{-1}(z)$ where K_{MJ}^{-1} is the inverse of $K_{JR} = z_i z_n G_{iJRn}$. Dunn (1994) obtained the closed form expressions for elliptical cylindrical inclusion or thin-disc inclusion embedded in a transversely isotropic matrix. For more general inclusion shapes and material symmetries, Eq. (A3) can be evaluated numerically as follows: (1) Compute ξ_1 and ξ_2 from ξ_3 and θ; (2) compute z_1, z_2 and z_3 from ξ_1, ξ_2 and ξ_3; (3) compute J_{MJin}; (4) evaluate the integral to get S_{MnAb}. Step (4) usually requires numerical integration.

References

Benveniste, Y., 1994. Exact connections between polycrystal and crystal properties in two-dimensional polycrystalline aggregates. Proc. R. Soc. Lond. A 447, 1–22.

Benveniste, Y., Dvorak, G.J., Chen, T., 1991. On diagonal and elastic symmetry of the approximate effective stiffness tensor of heterogeneous media. J. Mech. Phys. Solids 39, 927–946.

Berlincourt, D., Jaffe, H., 1958. Elastic and piezoelectric coefficients of single-crystal barium titanate. Phys. Rev. B 111, 143–148.

Bisegna, P., Luciano, R., 1996. Variational bounds for the overall properties of piezoelectric composites. J. Mech. Phys. Solids 44, 583–602.

Bunge, H., 1982. Texture analysis in Materials Science. Butterworths, London.

Dunn, M.L., 1994. Electroelastic Green's functions for transversely isotropic piezoelectric media and their application to the solution of inclusion and inhomogeneity problems. Int. J. Engr. Sci. 32, 119–131.

Dunn, M.L., 1995. Effects of grain shape anisotropy, porosity, and microcracks on the elastic and dielectric constants of polycrystalline piezoelectric ceramics. Journal of Applied Physics 78, 1533–1542.

Dunn, M.L., Taya, M., 1993. An analysis of composite materials containing ellipsoidal piezoelectric inhomogeneities. Proceedings of the Royal Society of London A 443, 265–287.

Dunn, M.L., Wienecke, H.A., 1997. Inclusions and inhomogeneities in transversely isotropic piezoelectric solids. Int. J. Solids Struct. 34, 3571–3582.

Eshelby, J.D., 1957. The determination of the elastic field of an ellipsoidal inclusion, and related problems. Proceedings of the Royal Society of London A241, 376–396.

Ferrari, M., Johnson, G.C., 1988. The equilibrium properties of a 6 mm polycrystal exhibiting transverse isotropy. J. Appl. Phys. 63, 4460–4468.

Hashin, Z., Shtrikman, T., 1962. A variational approach to the elastic behavior of polycrystals. J. Mech. Phys. Solids 10, 343–352.

Hashin, Z., Shtrikman, T., 1963. A variational approach to the theory of the elastic behavior of multiphase materials. J. Mech. Phys. Solids 11, 127–140.

Hori, M., Nemat-Nasser, S., 1998. Universal bounds for effective piezoelectric moduli. Mechanics of Materials 30, 1–30.

Li, J.Y., 1999. On micromechanics approximation for the effective thermoelastic moduli of multi-phase composite materials. Mechanics of Materials 31, 149–159.

Li, J.Y., Dunn, M.L., 1998a. Variational bounds for the effective moduli of heterogeneous piezoelectric solids, submitted.

Li, J.Y., Dunn, M.L., 1998b. Anisotropic inclusion and inhomogeneity problems. Philosophical Magazine A 77, 1341–1350.

Li, J.Y., Dunn, M.L., Ledbetter, H., 1999. Thermoelectroelastic moduli of textured piezoelectric poly-crystals: exact solutions and bounds for film textures, Journal of Applied Physics, accepted.

Lu, Y., Hoelzer, D.T., Schulze, W.A., Tuttle, B., Potter, B.G., 1996. Grain-oriented ferroelectric bismuth titanate thin film prepared from acetate precursor. Materials Science and Engineering B 39, 41–47.

Marutake, M., 1956. A calculation of physical constants of ceramic barium titanate. Journal of the Physical Society of Japan 11, 807–814.

Nye, J.F., 1957. Physical Properties of Crystals. Oxford University Press, Oxford, UK.

Olson, T., Avellaneda, M., 1992. Effective dielectric and elastic constants of piezoelectric polycrystals. J. Appl. Phys. 71, 4455–4464.

Press, W.H., Teukolsky, S.A., Vetterling, W.T., Flannery, B.P., 1992. Numerical Recipes in FORTRAN, 2nd ed. Cambridge University Press.

Reuss, A., 1929. Berechnung der Fliessgrenze von Mischkristallen auf Grund der Plastizita tsbedingung ur Einkristalle. Zeitschrift fur angewandte Mathematik und Mechanik 9, 49–58.

Roe, R.J., 1965. Description of crystalline orientation in polycrystalline materials, III. General solution to pole figure inversion. J. App. Phys. 36, 2024–2031.

Sakashita, Y., Segawa, H., Tominaga, K., Okada, M., 1993. Dependence of electric properties on film thickness in $Pb(Zr_xTi_{1-x})O_3$ thin films produced by metalorganic chemical vapor deposition. Journal of Applied Physics 73, 7857–7863.

Stemmer, S., Streiffer, S.K., Ernst, F., Ruhle, M., Hsu, W-Y., Raj, R., 1995. Domain configurations in ferroelectric $PbTiO_3$ thin films: the influence of substrate and film thickness. Solid State Ionics 75, 43–48.

Voigt, W., 1889. Ueber die Beziehung zwischen den beiden Elastizita tskonstanten isotroper Korper. Annalen der Physik 38, 573–587.

Walpole, L.J., 1969. On the overall elastic moduli of composite materials. J. Mech. Phys. Solids 17, 235–251.

Willis, J.R., 1977. Bounds and self-consistent estimates for the overall properties of anisotropic composites. J. Mech. Phys. Solids 25, 185–202.